Higher-order topological insulator in a modified Haldane-Hubbard model

Tian-Cheng Yi,[1] Hai-Qing Lin,[1,2] and Rubem Mondaini[1,*]
[1]*Beijing Computational Science Research Center, Beijing 100193, China*
[2]*School of Physics, Zhejiang University, Hangzhou, 310058, China*

(Received 21 December 2022; accepted 10 April 2023; published 20 April 2023)

We investigate the ground-state phase diagram of a modified spinless Haldane-Hubbard model, with broken threefold rotational symmetry, employing exact diagonalization calculations. The interplay of asymmetry, interactions, and topology gives rise to a rich phase diagram. The noninteracting limit of the Hamiltonian exhibits a higher-order topological insulator characterized by the existence of corner modes, in contrast to known chiral edge metallic states of the standard Haldane model. Our investigation demonstrates that these symmetry-protected states are robust to the presence of finite interactions. Furthermore, in certain regimes of parameters, we show that a topological Mott insulator exists in this model, where a nontrivial topological bulk coexists with an interaction-driven charge-density wave, whose emergence is characterized by a Z_2-symmetry breaking within the $3d$-Ising universality class.

DOI: 10.1103/PhysRevB.107.165135

I. INTRODUCTION

The discovery of topological insulators (TIs) and superconductors have attracted considerable attention, being extensively investigated in many different systems in recent years, such as in electronic [1,2] or photonic systems [3]. It has culminated with an overall scheme for classifying topological quantum matter depending on the symmetries of the related models [4]. A distinctive feature of TIs is the bulk-boundary correspondence: A d-dimensional TI exhibits topologically protected gapless states on its $(d-1)$-dimensional boundaries, mapped by the existence of a finite topological invariant in the bulk.

Even more recently, it has been noticed that in some cases, the protected modes are instead restricted to hinges or corners of the system [5,6]. This gave rise to the concept of higher-order topological insulators (HOTIs), which exhibit gapped $(d-1)$-dimensional boundaries while supporting gapless, topologically protected states on a lower $(d-n)$-dimensional boundary for $n \geqslant 2$. HOTIs have been experimentally observed in materials [7,8] or emulated in engineered platforms as mechanical or photonic metamaterials [9,10], or electric [11–13] and resonator circuits [14–17]. Theoretically, they have been classified in a variety of Hamiltonians, including modified versions of celebrated models such as the Su-Schrieffer-Heeger [18], Aubry-André-Harper [19], and Haldane models [20].

The latter [21] realizes a quantum anomalous Hall insulator featuring a topologically protected chiral state carrying a dissipationless current without an external magnetic field [22,23]. It has been generalized to understand the effects of interactions [24–31], disorder [32,33], and their combined interplay [34] in its topological properties. A common theme in these results is that, at half-filling, once interactions are sufficiently large to induce a finite local order parameter, protection of edge modes is absent, and trivial insulating phases ensue.

In the context of higher-order topology, decorated tight-binding models in the honeycomb lattice have been shown to support protected corner modes [35]. In particular, a generalization of the Haldane model that breaks its threefold rotational symmetry C_3 leads to a HOTI, provided that inversion symmetry is preserved [20]. Physically, this modification corresponds to a type of uniaxial strain in the system [36], whose characterization of first-order topological properties have been performed earlier [37,38].

The combination of these venues, interactions, and high-order topology has been much less explored. For example, recent results in electronic spinful Hamiltonians have demonstrated the formation of gapless, topologically protected spin excitations in corners of the lattice, whereas charge excitations are still gapped [39,40]; formation of gapless corner modes are also seen in either spin models [41,42] or extensions of the Bose-Hubbard model [43]. Yet, observation of interacting fermionic models featuring corner modes related to gapless charge excitations is currently lacking.

To fill this gap, we investigated a dimerized Haldane-Hubbard model, whose noninteracting counterpart was introduced in Ref. [20], to understand the robustness of second-order topological properties upon the inclusion of interactions. While many studies have classified the topological properties of the Haldane-Hubbard model [24–31], all these cases are limited to the first-order topology, i.e., to the appearance of protected *edge* states in certain regimes of parameters. By using exact diagonalization methods, we uncover the presence of an interacting HOTI, characterizing the formation of protected *corner* modes.

As a by-product of our analysis, we demonstrate the existence of a genuine topological Mott insulator (TMI) in this

*rmondaini@csrc.ac.cn

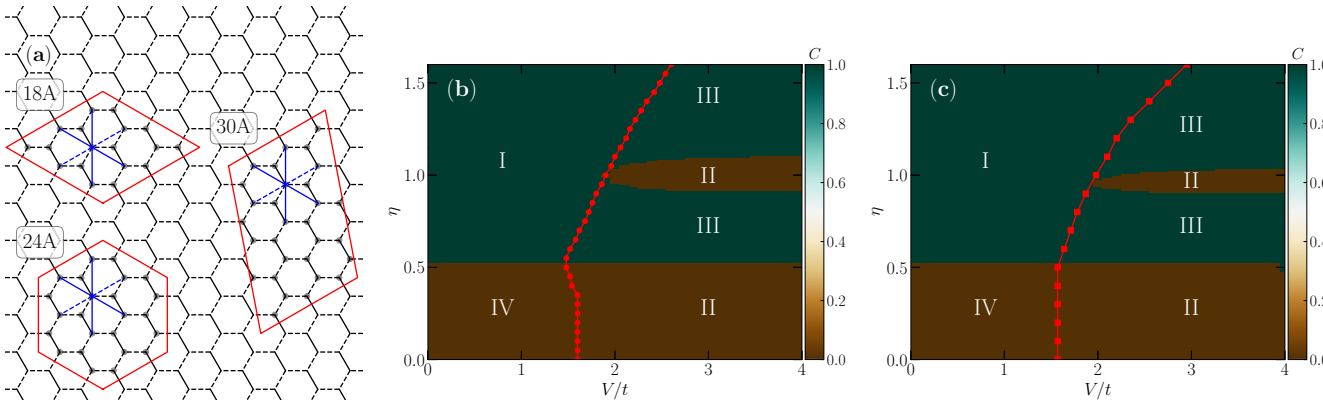

FIG. 1. (a) Schematic representation of the lattice clusters used in the ED calculations: 18A, 24A, and 30A. Solid and dashed lines represent the bonds for different hopping amplitudes between the nearest (black) and next-nearest (blue) neighbor sites. For clarity, the latter is just depicted for a single site in each cluster. Red solid lines give the cluster boundaries; open and periodic boundary conditions are used in the calculations. (b) and (c) The phase diagrams obtained for clusters 24A and 30A, respectively. The colors give the value of the (quantized) Chern number, and the connected markers the location of the CDW transition marked by the fidelity susceptibility χ_F. Different phases numbered I to IV, are labeled in the text. In particular, phase IV is the interacting HOTI, adiabatically connected to its $V = 0$ counterpart [20].

model [44], that is, a regime in the parameters in which both insulating behavior stemming from increasing interactions and nontrivial topological properties in the ground-state concomitantly occur. TMIs have a long history of research with often conflicting results: The existence of interaction-driven TMIs has been previously argued [45–53], while other results using unbiased methods [54–58] dispute some of the claims. An exception is the two-dimensional system featuring quadratic band crossings and weak interactions [59–65], but here such characterization is unambiguous. On top of that, since the onset of the TMI is manifested by the emergence of charge order, we show that the zero-temperature transition belongs to the $3d$-Ising universality class, owing to the Z_2-symmetry breaking of the corresponding order parameter.

II. MODEL AND QUANTITIES

We consider a modified Haldane-Hubbard model on a honeycomb lattice with the Hamiltonian,

$$\hat{\mathcal{H}} = -\sum_{\langle i,j\rangle} t_1^{ij}(\hat{c}_i^\dagger \hat{c}_j + \text{H.c.}) - \sum_{\langle\langle i,j\rangle\rangle} t_2^{ij}(e^{i\phi_{ij}}\hat{c}_i^\dagger \hat{c}_j + \text{H.c.}) + \Delta\sum_i (-1)^i \hat{n}_i + V\sum_{\langle ij\rangle} \hat{n}_i\hat{n}_j. \quad (1)$$

Here, $\hat{c}_i^\dagger$ ($\hat{c}_i$) is the fermion creation (annihilation) operator at site i, and $\hat{n}_i = \hat{c}_i^\dagger \hat{c}_i$ is the corresponding number operator. t_1^{ij} (t_2^{ij}) gives the nearest-neighbor (next-nearest-neighbor) hopping amplitude, and Δ is the staggered potential responsible for breaking the symmetry between the two sublattices of a honeycomb lattice. The next-nearest-neighbor hopping term has a complex phase $\phi_{ij} = +\phi(-\phi)$ for counter-clockwise (clockwise) hoppings and V describes the magnitude of a repulsive nearest-neighbor interaction.

When $t_1^{ij} = t_1$, $t_2^{ij} = t_2$, $\hat{\mathcal{H}}$ simplifies to the original homogeneous spinless Haldane-Hubbard model [24,26]. Alternatively, one can introduce a dimerization of both nearest and next-nearest neighbor hopping amplitudes along one preferential direction, as schematically represented in Fig. 1(a). These establish two types of bonds for each hopping term, whose amplitude is given, respectively, by $t_{1s,2s}$ and $t_{1d,2d}$.

By defining the dimerization strength, $\eta \equiv t_{1d}/t_{1s} \equiv t_{2d}/t_{2s}$, Ref. [20] showed that if departing from the homogeneous case with $\eta = 1$, a gap closes and reopens at $\eta = \pm 0.5$, such that for values $0.5 > \eta > -0.5$ the noninteracting ($V = 0$) Hamiltonian characterizes a HOTI, provided inversion symmetry is preserved (i.e., with $\Delta = 0$). This phase is described by having an associated zero value of the Chern number C, while yet harboring corner modes. Such a topological invariant is computed via the integration of the Berry curvature [66],

$$C = \int \frac{d\phi_x d\phi_y}{2\pi i}(\langle\partial_{\phi_x}\Psi_0^*|\partial_{\phi_y}\Psi_0\rangle - \langle\partial_{\phi_y}\Psi_0^*|\partial_{\phi_x}\Psi_0\rangle), \quad (2)$$

after introducing twisted boundary conditions $\{\phi_x, \phi_y\}$ [67] when obtaining the ground state $|\Psi_0\rangle$ of $\hat{\mathcal{H}}$. In practice, a sufficiently discretized version of Eq. (2) suffices [68], as has been shown to converge to a quantized Chern number in the same model [26,30,34].

In what follows, we investigate the low-lying spectral properties of $\hat{\mathcal{H}}$ by using exact diagonalization (ED) in finite clusters ranging from $N_s = 18$ to 30 sites, focusing the investigation at half-filling, i.e., $N_e \equiv \sum_i \langle\hat{n}_i\rangle = N_s/2$. A representation of the clusters used, all featuring the K high-symmetry point as a valid momentum value, is given in Fig. 1. Solid and dashed lines describe the different hopping amplitudes. When $\eta < 1$, they represent, respectively, the strong and weak bonds. For clarity, the (blue) solid and dashed lines denoting dimerized hopping amplitudes between next-nearest neighbor sites are expressed on a single site for each cluster; red lines give the cluster boundaries, which are chosen to be either open or periodic, depending on the quantities one is interested in.

On top of the topological properties, we characterize the formation of a charge-density wave (CDW) associated with a trivial Mott insulating (MI) behavior at sufficiently large V. For that, we quantify the $\mathbf{k} = 0$ CDW structure factor

[24,26,30,34,69],

$$S_{\rm CDW} \equiv \frac{1}{N}\sum_{i,j} C(\mathbf{r}_i - \mathbf{r}_j), \tag{3}$$

with density correlations,

$$C(\mathbf{r}_i - \mathbf{r}_j) = \langle (\hat{n}_i^a - \hat{n}_i^b)(\hat{n}_j^a - \hat{n}_j^b)\rangle, \tag{4}$$

where $\hat{n}_i^a$ and $\hat{n}_i^b$ are the number operators on sublattices a and b in the ith unit cell, respectively, and $N = N_s/2$ is the total number of unit cells. This quantity is extensive in N once a long-range CDW order sets in, tracking thus the formation of the corresponding local order parameter.

Lastly, we further quantify the fidelity susceptibility [70–73],

$$\chi_F = \frac{2}{N_s}\frac{1 - |\langle \Psi_0(V)|\Psi_0(V + dV)\rangle|}{dV^2}, \tag{5}$$

with $dV = 10^{-3}$ in our calculations, which identifies a continuous quantum phase transition through the location of an extensive peak in N_s in the region parameters of interest [24,74–77]. In the case of first-order topological phase transitions, as the CI-MI for $\eta = 1$, the fidelity susceptibility exhibits discontinuities so long as the lattice possesses the corresponding high-symmetry point where the closing of the excitation gap occurs [24,26,30].

Immediate verification of a first-order phase transition, invariably tied to the modification of the topological invariant, is obtained by the computation of the excitation (or many-body) gap:

$$\Delta_{\rm m} = E_1(N_s/2) - E_0(N_s/2), \tag{6}$$

which quantifies the energy difference between the two lowest eigenvalues of Eq. (1) for the studied filling factor $N_e = N_s/2$.

Other quantities, such as charge compressibilities and charge gaps, mainly used to identify the protected corner modes, are defined subsequently in the corresponding sections. In what follows, we choose $t_{2s}/t_{1s} = 0.2$, $\phi = \pi/2$ and establish $t_{1s} = t$ as the unit of energy. We also focus on the case that preserves inversion symmetry, i.e., $\Delta = 0$, since that is a precondition for the manifestation of a HOTI in this model [20]. Lastly, we narrow the investigation to the $\eta > 0$ regime.

III. RESULTS

A. Phase diagram

We start by describing the ground-state phase diagram of Eq. (1) in the space of parameters $\eta - V$ in Figs. 1(b) and 1(c), for the two largest clusters we study, 24A and 30A, respectively, using PBCs. We note the existence of four different phases based on the analysis of the quantized Chern number and the peak location of the fidelity susceptibility, which tracks the onset of CDW order when increasing the interaction strength:

(I) topological (Chern) insulator ($C = 1$, no CDW order);
(II) Mott insulator ($C = 0$, CDW order);
(III) topological Mott insulator ($C = 1$, CDW order);
(IV) higher-order topological insulator ($C = 0$, no CDW order).

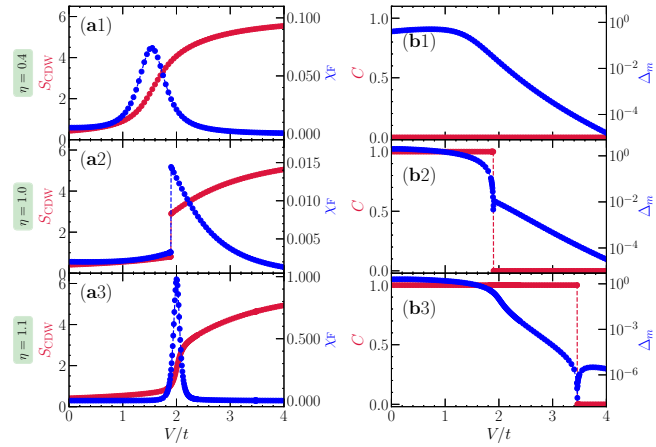

FIG. 2. (a1)–(a3) CDW structure factor (left) and fidelity susceptibility (right) along three cuts of the phase diagram, with $\eta = 0.4$; 1 and 1.1. (b1–b3). Corresponding results for the Chern number (left) and the excitation gap (right). Here we use the 24A cluster with PBCs.

In the absence of dimerization, $\eta = 1$, the transition between phases I and II describes the known results of the $\mathcal{C}_3$-symmetric Haldane-Hubbard model, namely, that a finite local order parameter is incompatible with nontrivial topology at half-filling [24,26]. That is, at a critical $V = V_c \simeq 2t$, the Chern insulator (I) gives way to a trivial Mott insulator (II). We further notice that this phase II defines a lobe that narrows in its η support when increasing the system size. While it is unclear whether phase II will be constrained to the $V > V_c$, $\eta = 1$ line in the thermodynamic limit, this trend makes apparent the robustness of phase III, namely, a nontrivial insulator ($C = 1$) that also exhibits CDW order. As far as we know, this is the first evidence of a topological Mott insulator in the Haldane-Hubbard model using unbiased methods.

For phase IV, we note that the noninteracting HOTI with $|\eta| < 0.5$ [20] adiabatically connects to its interacting counterpart. As expected, it exhibits a $C = 0$ topological invariant, but past $V/t \gtrsim 1.6$ is replaced by another trivial (i.e., $C = 0$) phase, which instead displays CDW order. This is again a manifestation of phase II, a trivial Mott insulator. Still, unlike in the case of $\eta = 1$, since there is no change of the topological invariant, the transition is second order, with a spontaneous Z_2 symmetry breaking.

Having presented the main features of the phase diagram, we now discuss details of how the different regions were inferred in the next two subsections.

B. Topological and Mott transitions

A remarkable feature that our phase diagram (Fig. 1) exposes is that the topological phase transition is not necessarily accompanied by a Mott one. Only in the case of the homogeneous (i.e., $\eta = 1$) Haldane-Hubbard model does this hold [24,26]. Finite hopping dimerization breaks such constraint, and Fig. 2 displays such dissociation. If we define the critical interaction that triggers a topological (Mott) transition at a given η as V_T (V_M), a known first-order phase transition at $V_T = V_M$ occurs in the homogeneous case, marked by a

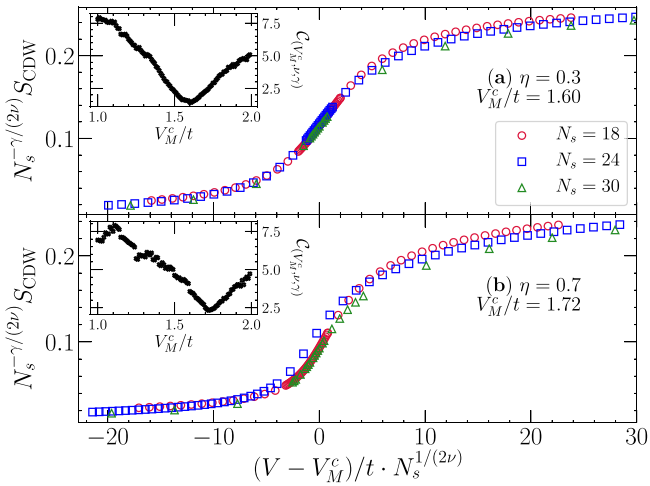

FIG. 3. Scaling behavior of $S_{\rm CDW}$ according to the scaling ansatz [Eq. (7)] with $3d$-Ising exponents $\gamma = 1.237075$ and $\nu = 0.629971$. (a) $\eta = 0.3$, describing the Mott transition within the $C = 0$ regime; (b) $\eta = 0.7$, Mott transition within the $C = 1$ phase. The insets show the corresponding values of the cost function (see text) for the scaling collapse as a function of V_M^c.

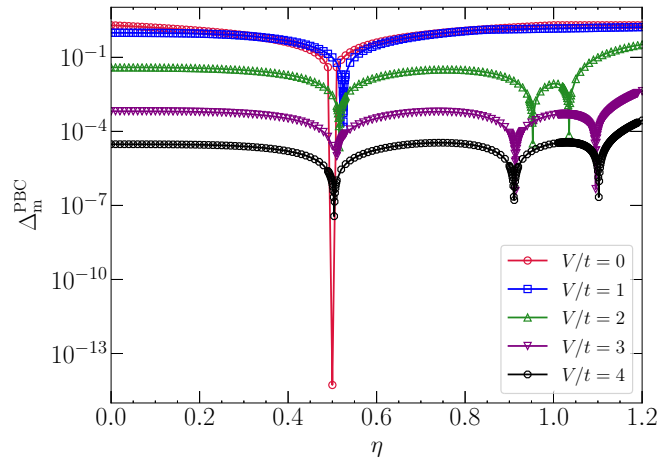

FIG. 4. Many-body gap $\Delta_{\rm m}$ dependence with different dimerization values along several cuts in the phase diagram with fixed interaction strengths. Here the 24A cluster is used with PBCs. The dips point to the critical value of η, where a bulk topological transition occurs.

simultaneous discontinuity of the structure factor and the fidelity susceptibility [Fig. 2(a2)]; this is also accompanied by a change of the Chern number, expressed by the closing of the excitation gap [Fig. 2(b2)]. In turn, if $\eta \neq 1$, $V_T \neq V_M$ in general. The topological transition is still marked by the location where $\Delta_{\rm m} = 0$ [e.g., see Fig. 2(b3)], which is no longer related to the point at which χ_F displays a peak [Fig. 2(a3)]. Finite-size effects are addressed in Appendix, showing that these results are qualitatively unchanged for other lattice sizes.

Since the Mott transition independently occurs from the topological character of the ground-state change, it can now reflect its typical second-order nature. The fidelity susceptibility becomes continuous, as is the CDW structure factor, where the ensuing charge ordering breaks a Z_2 symmetry. Consequently, this zero-temperature phase transition belongs to the (2+1)-d Ising universality class and $S_{\rm CDW}$ should obey the following scaling ansatz:

$$N_s^{-\gamma/2\nu} S_{\rm CDW} = g\big[(V - V_M^c) N_s^{1/2\nu}\big]. \tag{7}$$

In such universality class, the exponent ν related to the divergence of the correlation length is $\nu = 0.629971(4)$ while γ, related to the singular behavior of two-point correlation functions, is $\gamma = 1.237075(10)$ [78].

Figure 3 shows the scaling analysis using the three cluster sizes available and values of $\eta = 0.3$ and 0.7. We estimate the critical interaction V_M^c in the thermodynamic limit by the minimum value of a cost function that quantifies the scaling collapse. It is written as $\mathcal{C}_{(V_c,\nu,\gamma)} = (\sum_j |y_{j+1} - y_j|)/(\max\{y_j\} - \min\{y_j\}) - 1$ [79,80], where y_j are the values of $N_s^{-\gamma/2\nu} S_{\rm CDW}$ ordered according to their corresponding $(V - V_M^c) N_s^{1/2\nu}$'s (see insets in Fig. 3). A relatively good collapse and agreement with the expected critical exponents are obtained, despite having a maximal value of the linear lattice size $L = N_s^{1/2} \simeq 5.48$. For $\eta = 0.3$, the Chern number is zero across the whole range of interactions investigated (see Fig. 1), reflecting the aforementioned interacting HOTI to trivial Mott insulating transition. With $\eta = 0.7$, however, $C = 1$ irrespective of the V magnitude studied when entering the topological Mott insulating phase. This indicates that the $3d$-Ising universality class describes the Mott transition, whether or not the ground state exhibits a trivial Chern number.

C. Many-body gap, charge gap, and the HOTI

As mentioned above, direct evidence of the topological transition involving the change of the corresponding topological invariant is seen via the closing of the excitation gap. Figure 4 summarizes the dependence with the dimerization parameter η with different interaction magnitudes V. The noninteracting limit is well marked by $\Delta_{\rm m}^{\rm PBC} \to 0$ at $\eta = 0.5$, describing the HOTI to CI transition introduced in Ref. [20]. Within the interacting regime, various values of V lead to a gap closing occurring roughly at the same location, while if the interactions are sufficiently large, a double dip structure centered around the $\mathcal{C}_3$-symmetric Haldane-Hubbard model ($\eta = 1$) marks the trivial Mott insulating lobes described in the phase diagram (Fig. 1).

Although the excitation gap is sufficient to identify the regimes where the Chern number changes, it completely misses the characterization of the higher-order topological regime. This is evident if spanning the interactions with $\eta < 0.5$: C is always zero and $\Delta_{\rm m}$ remains finite across a wide range of interactions [see, e.g., Fig. 2(b1)]. Quantification of the HOTI and its corner modes relies thus on other metrics. In particular, in the context of interacting systems, one can no longer refer to such modes as gapless excitations in the single-particle spectrum. Instead, one expects its manifestation via the existence of gapless *charge excitations*. The relevant metric is the charge gap defined as

$$\Delta_{\rm c} = E_0(N_s/2 + 1) + E_0(N_s/2 - 1) - 2E_0(N_s/2), \tag{8}$$

which computes the difference in chemical potentials of adding and removing a single particle upon the half-filling

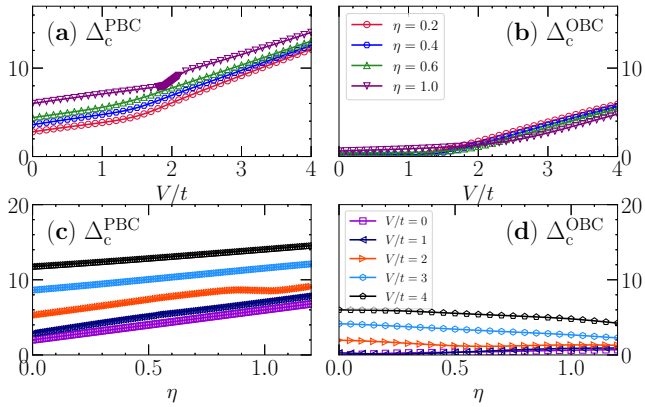

FIG. 5. Charge gap Δ_c dependence on V [(a) and (b)] and η [(c) and (d)], contrasting both PBC (left panels) and OBC (right) in the 24A cluster. While always finite, Δ_c^{OBC} is the smallest when $V \lesssim V_M$ and $\eta \lesssim 0.5$, a regime where the interacting HOTI phase is suggested.

$N_e = N_s/2$ we study. To understand the regimes where the HOTI occurs, we need thus to contrast the charge gaps on clusters employing both PBCs and OBCs. Only in the latter can a possible manifestation of corner modes take place.

Figure 5 characterizes this on the 24A cluster, showing that (i) for the same parameter's settings, the OBC charge gaps are always smaller than its PBC counterpart, despite being finite due to size effects; (ii) concerning its V dependence, Δ_c^{OBC} only steadily increases when $V \gtrsim V_M$, i.e., when charge ordering sets in, while at $\eta \lesssim 0.5$ and $V \lesssim V_M$ the smallest gaps are obtained—this is the regime where according to the phase diagram a HOTI manifests.

Although suggestive, such an analysis is superficial in establishing the existence of corner modes. Direct evidence can be put forward by defining the site-resolved compressibility,

$$K_c(i) = \frac{\partial \langle \hat{n}_i \rangle}{\partial \mu} \approx \frac{\langle \hat{n}_i \rangle_{N_e+1} - \langle \hat{n}_i \rangle_{N_e}}{\mu_+ - \mu_-}, \tag{9}$$

where $\mu_+ = E_0(N_e+1) - E_0(N_e)$ and $\mu_- = E_0(N_e) - E_0(N_e-1)$ are the chemical potentials of adding and removing a single charge, respectively. Similar analysis has been employed in the context of spin-corner modes in other interacting models exhibiting higher-order topology [40].

We report in Fig. 6 the lattice profile of compressibilities $K_c(i)$ in four representative points of the phase diagram for cluster 30A. While for parameters in phases I, II, and III $|K_c(i)| \simeq 0$ across the whole lattice, in phase IV, it is clear that much higher compressibilities are obtained for selected sites. This is direct evidence of the interacting HOTI in the modified Haldane-Hubbard model.

Two points are important to emphasize. While corner modes are essentially localized, these will always manifest a profile in real space, which poses challenges to its verification in small clusters (amenable to ED calculations). Second, a particularity that appears even in the $V = 0$ limit of the dimerized Haldane-Hubbard model highlighted in Ref. [20] is that by studying semi-infinite ribbons, protected in-gap modes for $0 < \eta < 0.5$ are only observed in the case where one employs

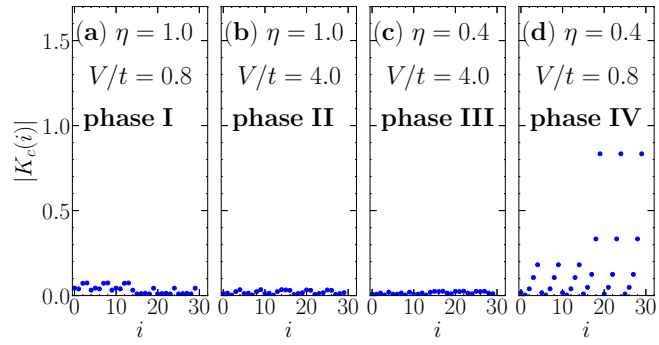

FIG. 6. The absolute value of the site-resolved charge compressibility in different phases, according to the phase diagram, for the 30A cluster. Here mixed (or cylindrical) boundary conditions are used (see text) and specific details with increasing interactions V and dimerization η can be seen at Figs. 7 and 8.

an OBC cut across the t_{1s} bonds (or strong bonds for $\eta < 1$). We follow a similar prescription here, defining mixed (or cylindrical) boundary conditions as schematically represented in Figs. 7 and 8 with the solid (PBC) and dashed (OBC) lines.

The transition from an interacting HOTI to the trivial Mott insulator under the scope of localized modes is shown in Fig. 7, for a fixed $\eta = 0.4$ and increasing interactions. It becomes apparent that the large compressibility at certain sites

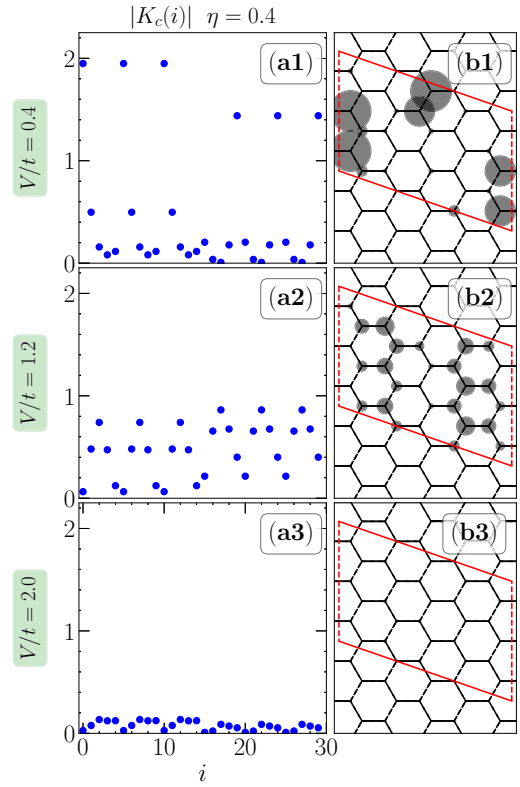

FIG. 7. The absolute value of the site-resolved charge compressibility with increasing interactions, $V/t = 0.4$, 1.2, and 2.0, in panels (a1)–(a3), with fixed $\eta = 0.4$. Panels (b1)–(b3) show the same data but are represented as markers in the 30A cluster whose size is proportional to the $|K_c(i)|$ value.

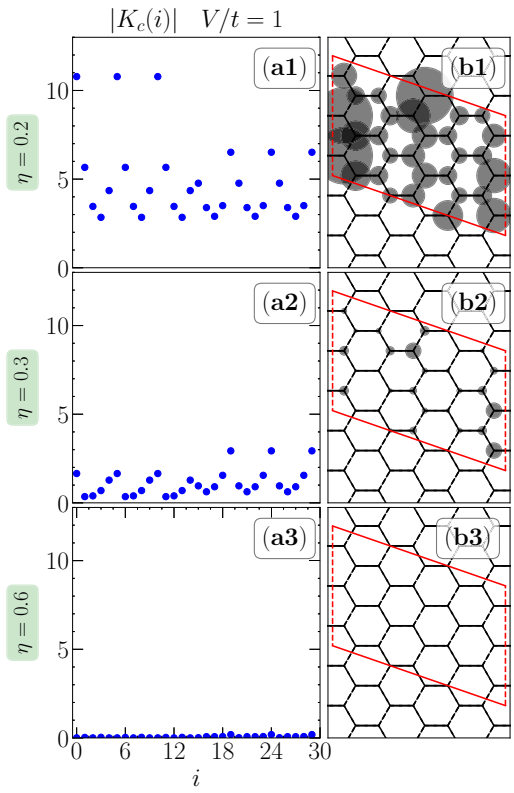

FIG. 8. Similar to Fig. 7, but with fixed interactions $V/t = 1$ and various dimerizations η, as marked.

is quickly suppressed once charge ordering, characteristic of the trivial Mott insulator, appears. Similarly, in Fig. 8, one can observe the interacting HOTI to CI transition with fixed interactions $V/t = 1$ and increasing η.

IV. SUMMARY AND OUTLOOK

Using exact calculations in small clusters, we show that a variant of the Haldane-Hubbard model displays a rich phase diagram, including unequivocal evidence of localized modes characteristic of high-order topology and the manifestation of a topological Mott insulator. The fundamental ingredient is the C_3-symmetry breaking dimerization of the hoppings, which allows the topological and Mott transitions to be dissociated in this model. In doing so, the transition to a charge-ordered phase turns continuous (in opposition to first order), whose universality class reflects the symmetry breaking of the CDW state.

This modification in the hoppings in the Haldane model was originally introduced in Ref. [20] as a way to unveil localized corner modes characteristic of second-order topology and is a common way to construct high-order topological insulators [5,6]. We show that the inclusion of interactions leads to a ground state adiabatically connected to it, generalizing the HOTI to the many-body realm. While exact calculations allow sufficient evidence for this characterization, the smallness of the clusters amenable to calculations and the fact the gapless charge excitations are not localized on a single site makes finite-size effects potentially relevant. Studying this model in a semi-infinite ribbon geometry, which, depending on how the OBCs are introduced, can harbor in-gap states in the noninteracting limit, is friendly to other techniques, including the infinite density matrix renormalization group [81,82]. We envision the characterization of the HOTI phase, especially its boundaries to either the CI or the trivial Mott insulator, to be particularly sharp owing to the mitigated finite-size effects. We leave such an investigation to future studies. Further characterization similar to the ones we conduct here also can be put forward in the case of the two-dimensional Su-Schrieffer-Heeger model, whose dimerization sets a natural condition for the emergence of higher-order topology [18,83,84]. The study of its robustness upon including interactions is currently largely unexplored.

ACKNOWLEDGMENTS

We acknowledge support from the National Natural Science Foundation of China (NSFC) Grant No. NSAF-U2230402. H.-Q.L. is supported by NSFC Grant No. 12088101; R.M. acknowledges NSFC Grants No. 11974039, No. 12050410263, No. 12111530010, and No. 12222401.

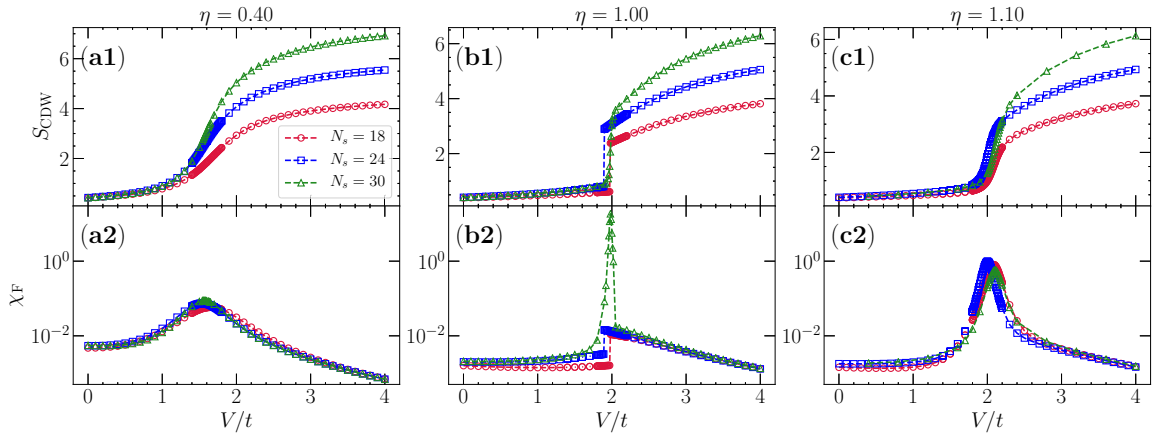

FIG. 9. (a1)–(c1) CDW structure factor dependence with the interactions V and different η's ($\eta = 0.4$, 1 and 1.1, respectively), contrasting the different system sizes we employ under PBCs. (a2)–(c2) The same dependence but for fidelity susceptibility χ_F. Discontinuities in both quantities are only seen in the homogeneous case $\eta = 1$, signaling the Mott transition to be first order.

Computations were performed on the Tianhe-2JK at the Beijing Computational Science Research Center.

APPENDIX: FINITE-SIZE EFFECTS IN THE MOTT TRANSITION

The main text shows the fidelity susceptibility and the charge-density-wave structure factor for cuts in the phase diagram and a single system size, $N_s = 24$ (Fig. 2). Figure 9 generalizes those results for the different system sizes studied. The general conclusions hold: Discontinuities in χ_F and S_{CDW} are obtained in the $\eta = 1$ (homogeneous) case, associated with the simultaneous Mott and topological transitions, whereas other values of η show behavior typical of second-order phase transitions for the charge-ordered transition.

[1] M. Z. Hasan and C. L. Kane, *Colloquium*: Topological insulators, Rev. Mod. Phys. **82**, 3045 (2010).

[2] X.-L. Qi and S.-C. Zhang, Topological insulators and superconductors, Rev. Mod. Phys. **83**, 1057 (2011).

[3] T. Ozawa, H. M. Price, A. Amo, N. Goldman, M. Hafezi, L. Lu, M. C. Rechtsman, D. Schuster, J. Simon, O. Zilberberg, and I. Carusotto, Topological photonics, Rev. Mod. Phys. **91**, 015006 (2019).

[4] C.-K. Chiu, J. C. Y. Teo, A. P. Schnyder, and S. Ryu, Classification of topological quantum matter with symmetries, Rev. Mod. Phys. **88**, 035005 (2016).

[5] W. A. Benalcazar, B. A. Bernevig, and T. L. Hughes, Quantized electric multipole insulators, Science **357**, 61 (2017).

[6] F. Schindler, A. M. Cook, M. G. Vergniory, Z. Wang, S. S. P. Parkin, B. A. Bernevig, and T. Neupert, Higher-order topological insulators, Sci. Adv. **4**, eaat0346 (2018).

[7] F. Schindler, Z. Wang, M. G. Vergniory, A. M. Cook, A. Murani, S. Sengupta, A. Y. Kasumov, R. Deblock, S. Jeon, I. Drozdov, H. Bouchiat, S. Guéron, A. Yazdani, B. A. Bernevig, and T. Neupert, Higher-order topology in bismuth, Nat. Phys. **14**, 918 (2018).

[8] C. Yue, Y. Xu, Z. Song, H. Weng, Y.-M. Lu, C. Fang, and X. Dai, Symmetry-enforced chiral hinge states and surface quantum anomalous Hall effect in the magnetic axion insulator $Bi_{2-x}Sm_xSe_3$, Nat. Phys. **15**, 577 (2019).

[9] M. Serra-Garcia, V. Peri, R. Süsstrunk, O. R. Bilal, T. Larsen, L. G. Villanueva, and S. D. Huber, Observation of a phononic quadrupole topological insulator, Nature (London) **555**, 342 (2018).

[10] M. Li, D. Zhirihin, M. Gorlach, X. Ni, D. Filonov, A. Slobozhanyuk, A. Alù, and A. B. Khanikaev, Higher-order topological states in photonic kagome crystals with long-range interactions, Nat. Photonics **14**, 89 (2020).

[11] S. Imhof, C. Berger, F. Bayer, J. Brehm, L. W. Molenkamp, T. Kiessling, F. Schindler, C. H. Lee, M. Greiter, T. Neupert, and R. Thomale, Topolectrical-circuit realization of topological corner modes, Nat. Phys. **14**, 925 (2018).

[12] W. Zhang, D. Zou, Q. Pei, W. He, J. Bao, H. Sun, and X. Zhang, Experimental Observation of Higher-Order Topological Anderson Insulators, Phys. Rev. Lett. **126**, 146802 (2021).

[13] B. Lv, R. Chen, R. Li, C. Guan, B. Zhou, G. Dong, C. Zhao, Y. Li, Y. Wang, H. Tao, J. Shi, and D.-H. Xu, Realization of quasicrystalline quadrupole topological insulators in electrical circuits, Commun. Phys. **4**, 108 (2021).

[14] C. W. Peterson, W. A. Benalcazar, T. L. Hughes, and G. Bahl, A quantized microwave quadrupole insulator with topologically protected corner states, Nature (London) **555**, 346 (2018).

[15] H. Xue, Y. Yang, F. Gao, Y. Chong, and B. Zhang, Acoustic higher-order topological insulator on a kagome lattice, Nat. Mater. **18**, 108 (2019).

[16] X. Ni, M. Weiner, A. Alù, and A. B. Khanikaev, Observation of higher-order topological acoustic states protected by generalized chiral symmetry, Nat. Mater. **18**, 113 (2019).

[17] S. S. Yamada, T. Li, M. Lin, C. W. Peterson, T. L. Hughes, and G. Bahl, Bound states at partial dislocation defects in multipole higher-order topological insulators, Nat. Commun. **13**, 2035 (2022).

[18] X.-J. Luo, X.-H. Pan, C.-X. Liu, and X. Liu, Higher-order topological phases emerging from Su-Schrieffer-Heeger stacking, Phys. Rev. B **107**, 045118 (2023).

[19] Q.-B. Zeng, Y.-B. Yang, and Y. Xu, Higher-order topological insulators and semimetals in generalized Aubry-André-Harper models, Phys. Rev. B **101**, 241104(R) (2020).

[20] B. Wang, X. Zhou, H. Lin, and A. Bansil, Higher-order topological insulator phase in a modified Haldane model, Phys. Rev. B **104**, L121108 (2021).

[21] F. D. M. Haldane, Model for a Quantum Hall Effect without Landau Levels: Condensed-Matter Realization of the "Parity Anomaly", Phys. Rev. Lett. **61**, 2015 (1988).

[22] C.-X. Liu, S.-C. Zhang, and X.-L. Qi, The quantum anomalous Hall effect: Theory and experiment, Annu. Rev. Condens. Matter Phys. **7**, 301 (2016).

[23] C.-Z. Chang, C.-X. Liu, and A. H. MacDonald, *Colloquium*: Quantum anomalous hall effect, Rev. Mod. Phys. **95**, 011002 (2023).

[24] C. N. Varney, K. Sun, M. Rigol, and V. Galitski, Interaction effects and quantum phase transitions in topological insulators, Phys. Rev. B **82**, 115125 (2010).

[25] L. Wang, H. Shi, S. Zhang, X. Wang, X. Dai, and X. C. Xie, Charge-density-wave and topological transitions in interacting Haldane model, arXiv:1012.5163.

[26] C. N. Varney, K. Sun, M. Rigol, and V. Galitski, Topological phase transitions for interacting finite systems, Phys. Rev. B **84**, 241105(R) (2011).

[27] T. I. Vanhala, T. Siro, L. Liang, M. Troyer, A. Harju, and P. Törmä, Topological Phase Transitions in the Repulsively Interacting Haldane-Hubbard Model, Phys. Rev. Lett. **116**, 225305 (2016).

[28] J. Imriška, L. Wang, and M. Troyer, First-order topological phase transition of the Haldane-Hubbard model, Phys. Rev. B **94**, 035109 (2016).

[29] I. S. Tupitsyn and N. V. Prokof'ev, Phase diagram topology of the Haldane-Hubbard-Coulomb model, Phys. Rev. B **99**, 121113(R) (2019).

[30] C. Shao, E. V. Castro, S. Hu, and R. Mondaini, Interplay of local order and topology in the extended Haldane-Hubbard model, Phys. Rev. B **103**, 035125 (2021).

[31] P. Mai, B. E. Feldman, and P. W. Phillips, Topological Mott insulator at quarter filling in the interacting Haldane model, Phys. Rev. Res. **5**, 013162 (2023).

[32] P. V. Sriluckshmy, K. Saha, and R. Moessner, Interplay between topology and disorder in a two-dimensional semi-Dirac material, Phys. Rev. B **97**, 024204 (2018).

[33] M. Gonçalves, P. Ribeiro, and E. V. Castro, The Haldane model under quenched disorder, arXiv:1807.11247.

[34] T.-C. Yi, S. Hu, E. V. Castro, and R. Mondaini, Interplay of interactions, disorder, and topology in the Haldane-Hubbard model, Phys. Rev. B **104**, 195117 (2021).

[35] Y. Xue, H. Huan, B. Zhao, Y. Luo, Z. Zhang, and Z. Yang, Higher-order topological insulators in two-dimensional Dirac materials, Phys. Rev. Res. **3**, L042044 (2021).

[36] V. M. Pereira, A. H. Castro Neto, and N. M. R. Peres, Tight-binding approach to uniaxial strain in graphene, Phys. Rev. B **80**, 045401 (2009).

[37] Y.-H. Ho, E. V. Castro, and M. A. Cazalilla, Haldane model under nonuniform strain, Phys. Rev. B **96**, 155446 (2017).

[38] M. Mannaï and S. Haddad, Strain tuned topology in the Haldane and the modified Haldane models, J. Phys.: Condens. Matter **32**, 225501 (2020).

[39] K. Kudo, T. Yoshida, and Y. Hatsugai, Higher-Order Topological Mott Insulators, Phys. Rev. Lett. **123**, 196402 (2019).

[40] Y. Otsuka, T. Yoshida, K. Kudo, S. Yunoki, and Y. Hatsugai, Higher-order topological mott insulator on the pyrochlore lattice, Sci. Rep. **11**, 20270 (2021).

[41] O. Dubinkin and T. L. Hughes, Higher-order bosonic topological phases in spin models, Phys. Rev. B **99**, 235132 (2019).

[42] J. Guo, J. Sun, X. Zhu, C.-A. Li, H. Guo, and S. Feng, Quantum Monte Carlo study of topological phases on a spin analogue of Benalcazar–Bernevig–Hughes model, J. Phys.: Condens. Matter **34**, 035603 (2021).

[43] J. Bibo, I. Lovas, Y. You, F. Grusdt, and F. Pollmann, Fractional corner charges in a two-dimensional superlattice Bose-Hubbard model, Phys. Rev. B **102**, 041126(R) (2020).

[44] S. Rachel, Interacting topological insulators: a review, Rep. Prog. Phys. **81**, 116501 (2018).

[45] S. Raghu, X.-L. Qi, C. Honerkamp, and S.-C. Zhang, Topological Mott Insulators, Phys. Rev. Lett. **100**, 156401 (2008).

[46] J. Wen, A. Rüegg, C.-C. Joseph Wang, and G. A. Fiete, Interaction-driven topological insulators on the kagome and the decorated honeycomb lattices, Phys. Rev. B **82**, 075125 (2010).

[47] J. C. Budich, R. Thomale, G. Li, M. Laubach, and S.-C. Zhang, Fluctuation-induced topological quantum phase transitions in quantum spin-Hall and anomalous-Hall insulators, Phys. Rev. B **86**, 201407(R) (2012).

[48] A. Dauphin, M. Müller, and M. A. Martin-Delgado, Rydberg-atom quantum simulation and Chern-number characterization of a topological Mott insulator, Phys. Rev. A **86**, 053618 (2012).

[49] C. Weeks and M. Franz, Interaction-driven instabilities of a Dirac semimetal, Phys. Rev. B **81**, 085105 (2010).

[50] L. Wang, X. Dai, and X. C. Xie, Interaction-induced topological phase transition in the Bernevig-Hughes-Zhang model, Europhys. Lett. **98**, 57001 (2012).

[51] A. Rüegg and G. A. Fiete, Topological insulators from complex orbital order in transition-metal oxides heterostructures, Phys. Rev. B **84**, 201103(R) (2011).

[52] K.-Y. Yang, W. Zhu, D. Xiao, S. Okamoto, Z. Wang, and Y. Ran, Possible interaction-driven topological phases in (111) bilayers of $LaNiO_3$, Phys. Rev. B **84**, 201104(R) (2011).

[53] T. Yoshida, R. Peters, S. Fujimoto, and N. Kawakami, Characterization of a Topological Mott Insulator in One Dimension, Phys. Rev. Lett. **112**, 196404 (2014).

[54] N. A. García-Martínez, A. G. Grushin, T. Neupert, B. Valenzuela, and E. V. Castro, Interaction-driven phases in the half-filled spinless honeycomb lattice from exact diagonalization, Phys. Rev. B **88**, 245123 (2013).

[55] M. Daghofer and M. Hohenadler, Phases of correlated spinless fermions on the honeycomb lattice, Phys. Rev. B **89**, 035103 (2014).

[56] J. Motruk, A. G. Grushin, F. de Juan, and F. Pollmann, Interaction-driven phases in the half-filled honeycomb lattice: An infinite density matrix renormalization group study, Phys. Rev. B **92**, 085147 (2015).

[57] S. Capponi and A. M. Läuchli, Phase diagram of interacting spinless fermions on the honeycomb lattice: A comprehensive exact diagonalization study, Phys. Rev. B **92**, 085146 (2015).

[58] D. D. Scherer, M. M. Scherer, and C. Honerkamp, Correlated spinless fermions on the honeycomb lattice revisited, Phys. Rev. B **92**, 155137 (2015).

[59] K. Sun, H. Yao, E. Fradkin, and S. A. Kivelson, Topological Insulators and Nematic Phases from Spontaneous Symmetry Breaking in 2D Fermi Systems with a Quadratic Band Crossing, Phys. Rev. Lett. **103**, 046811 (2009).

[60] J. M. Murray and O. Vafek, Renormalization group study of interaction-driven quantum anomalous Hall and quantum spin Hall phases in quadratic band crossing systems, Phys. Rev. B **89**, 201110(R) (2014).

[61] J. W. F. Venderbos, M. Manzardo, D. V. Efremov, J. van den Brink, and C. Ortix, Engineering interaction-induced topological insulators in a $\sqrt{3} \times \sqrt{3}$ substrate-induced honeycomb superlattice, Phys. Rev. B **93**, 045428 (2016).

[62] H.-Q. Wu, Y.-Y. He, C. Fang, Z. Y. Meng, and Z.-Y. Lu, Diagnosis of Interaction-driven Topological Phase via Exact Diagonalization, Phys. Rev. Lett. **117**, 066403 (2016).

[63] W. Zhu, S.-S. Gong, T.-S. Zeng, L. Fu, and D. N. Sheng, Interaction-Driven Spontaneous Quantum Hall Effect on a Kagome Lattice, Phys. Rev. Lett. **117**, 096402 (2016).

[64] O. Vafek and K. Yang, Many-body instability of Coulomb interacting bilayer graphene: Renormalization group approach, Phys. Rev. B **81**, 041401(R) (2010).

[65] J. Wang, C. Ortix, J. van den Brink, and D. V. Efremov, Fate of interaction-driven topological insulators under disorder, Phys. Rev. B **96**, 201104(R) (2017).

[66] Q. Niu, D. J. Thouless, and Y.-S. Wu, Quantized hall conductance as a topological invariant, Phys. Rev. B **31**, 3372 (1985).

[67] D. Poilblanc, Twisted boundary conditions in cluster calculations of the optical conductivity in two-dimensional lattice models, Phys. Rev. B **44**, 9562 (1991).

[68] T. Fukui, Y. Hatsugai, and H. Suzuki, Chern numbers in discretized Brillouin zone: Efficient method of computing (spin) Hall conductances, J. Phys. Soc. Jpn. **74**, 1674 (2005).

[69] C. Shao, P. D. Sacramento, and R. Mondaini, Photoinduced anomalous Hall effect in the interacting Haldane model: Targeting topological states with pump pulses, Phys. Rev. B **104**, 125129 (2021).

[70] P. Zanardi and N. Paunković, Ground state overlap and quantum phase transitions, Phys. Rev. E **74**, 031123 (2006).

[71] L. Campos Venuti and P. Zanardi, Quantum Critical Scaling of the Geometric Tensors, Phys. Rev. Lett. **99**, 095701 (2007).

[72] P. Zanardi, P. Giorda, and M. Cozzini, Information-Theoretic Differential Geometry of Quantum Phase Transitions, Phys. Rev. Lett. **99**, 100603 (2007).

[73] W.-L. You, Y.-W. Li, and S.-J. Gu, Fidelity, dynamic structure factor, and susceptibility in critical phenomena, Phys. Rev. E **76**, 022101 (2007).

[74] M.-F. Yang, Ground-state fidelity in one-dimensional gapless models, Phys. Rev. B **76**, 180403(R) (2007).

[75] C. J. Jia, B. Moritz, C.-C. Chen, B. S. Shastry, and T. P. Devereaux, Fidelity study of the superconducting phase diagram in the two-dimensional single-band Hubbard model, Phys. Rev. B **84**, 125113 (2011).

[76] R. Mondaini, P. Nikolić, and M. Rigol, Mott-insulator–to–superconductor transition in a two-dimensional superlattice, Phys. Rev. A **92**, 013601 (2015).

[77] X. Jin, Y. Liu, R. Mondaini, and M. Rigol, Charge excitations across a superconductor-insulator transition, Phys. Rev. B **106**, 245117 (2022).

[78] A. Pelissetto and E. Vicari, Critical phenomena and renormalization-group theory, Phys. Rep. **368**, 549 (2002).

[79] J. Šuntajs, J. Bonča, T. Prosen, and L. Vidmar, Ergodicity breaking transition in finite disordered spin chains, Phys. Rev. B **102**, 064207 (2020).

[80] R. Mondaini, S. Tarat, and R. T. Scalettar, Universality and critical exponents of the fermion sign problem, arXiv:2207.09026.

[81] S. R. White, Density Matrix Formulation for Quantum Renormalization Groups, Phys. Rev. Lett. **69**, 2863 (1992).

[82] J. A. Kjäll, M. P. Zaletel, R. S. K. Mong, J. H. Bardarson, and F. Pollmann, Phase diagram of the anisotropic spin-2 XXZ model: Infinite-system density matrix renormalization group study, Phys. Rev. B **87**, 235106 (2013).

[83] Y. Otaki and T. Fukui, Higher-order topological insulators in a magnetic field, Phys. Rev. B **100**, 245108 (2019).

[84] C.-A. Li, S.-B. Zhang, J. C. Budich, and B. Trauzettel, Transition from metal to higher-order topological insulator driven by random flux, Phys. Rev. B **106**, L081410 (2022).